SCIENCE CHINA
Chemistry

• ARTICLES •

November 2014 Vol.57 No.11: 1570–1578
doi: 10.1007/s11426-014-5123-x

Effect of surface area and heteroatom of porous carbon materials on electrochemical capacitance in aqueous and organic electrolytes

WANG RuTao[1,2,3], LANG JunWei[1] & YAN XingBin[1,2*]

[1]*Laboratory of Clean Energy Chemistry and Materials, Lanzhou Institute of Chemical Physics, Chinese Academy of Sciences, Lanzhou 730000, China*
[2]*State Key Laboratory of Solid Lubrication, Lanzhou Institute of Chemical Physics, Chinese Academy of Sciences, Lanzhou 730000, China*
[3]*University of Chinese Academy of Sciences, Beijing 100080, China*

Received March 12, 2014; accepted March 27, 2014; published online June 10, 2014

A series of porous carbon materials with wide range of specific surface areas and different heteroatom contents had been prepared using polyaniline as carbon precursor and KOH as an activating agent. Effect of surface area and heteroatom of porous carbon materials on specific capacitance was investigated thoroughly in two typical aqueous KOH and organic 1-butyl-3-methylimidazolium tetrafluoroborate/acetonitirle electrolytes. The different trends of capacitance performance were observed in these two electrolytes. Electrochemical analyses suggested that the presence of faradaic interactions on heteroatom-enriched carbon materials in organic environment is less significant than that observed in aqueous electrolytes. Thus, in aqueous electrolyte, a balance between surface area and heteroatom content of activated porous carbon would be found to develop a supercapacitor with high energy density. In organic electrolyte, the capacitance performance of porous carbon is strongly dependent on the surface area. The results may be useful for the design of porous carbon-based supercapacitor with the desired capacitive performance in aqueous and organic electrolytes.

porous carbon, supercapacitor, heteroatom, KOH activation, organic electrolyte, KOH electrolyte

1 Introduction

Porous carbon materials, which are the first candidates as the electrode materials for supercapacitor, have attracted tremendous attention owing to an array of their exceptional characteristics, including low cost, easy availability, and outstanding electrochemical stability [1–3]. Traditionally, the energy storage of porous carbon materials is mainly attributed to the electric double-layer capacitance (EDLC) which is based on the interfacial electrostatic adsorption between the electrode and electrolyte. Thus, the specific capacitance of porous carbon materials falls into the influence of many factors such as pore size distribution (PSD), specific surface area (SSA) and conductivity [2, 3].

Much effort has been devoted to numerous porous carbon materials with high SSA and controllable PSD through various chemical/physical methods and well-established experimental parameters [4–12]. Most important advantages of these approaches are that the as-obtained porous carbon materials have rather high SSA and well-controlled PSD. Narrow PSD facilitates the study of the relationship between pore structure and electrolyte ions [13–17]. However, a wide scope of carbon materials, especially commercial activated carbons, usually have different SSAs and wide PSD [6, 7, 10–12, 18]. More complete studies are still needed. Recently, Zhang and co-workers [19] proposed a simple and reliable model for estimating specific capacitance of porous carbon materials with the wide PSD and found that the specific capacitance performance of carbon materials was linear with the effective SSA. It should be mentioned that this model is based on the pure ionic liquids.

*Corresponding author (email: xbyan@licp.cas.cn)

It is still unknown whether this model works effectively in aqueous or other organic electrolytes.

More or less heteroatom remains in or is introduced on the porous carbon during the preparation process [20–26]. These heteroatoms (e.g., O and N), as the form of functional groups, exhibit a so-called pseudocapacitance which is related to redox reactions involving different oxidation states within an operational potential window [3, 20, 27–30]. Recent studies showed that pseudocapacitance from heteroatom functional groups could provide a supplementary contribution to a dominant double-layer capacitance [27–33]. Even, some heteroatom enriched carbon materials with low SSA have the high capacitance values which are mainly contributed from heteroatom functional groups [34, 35]. This means that the capacitance performance of porous carbon depends on the SSA and heteroatom content. For most of chemical/physical preparation methods, high SSA of porous carbon material is usually obtained at the high temperature, while heteroatoms are often not stable and their contents reduce in this stage [20, 22, 25, 36–38]. For most of porous carbon materials, large double-layer capacitance and high pseudocapacitance both could not be obtained. Therefore, thorough investigation is much needed to explore the controlling of both SSA and heteroatom content of porous carbons for more effective materials designed with better capacitance performances.

Polyaniline (PANi) is an ideal carbon precursor for synthesis of activated carbon due to uniformly distributed heteroatom source (N atom: about 15 wt%) in its structure. Some elegant works have been reported in this regards using the PANi prepared porous carbon through the chemical activation for application in supercapacitor, Li-ion batteries, and gas capture [39–41]. The advantages of PANi prepared activated carbons are visible due to their well-developed pore structure and tunable heteroatom content.

In this work, various porous carbon materials with different SSAs and heteroatom contents were prepared through a facile and widely used KOH activation method through using PANi as carbon source and adjusting the activation temperature. Then, using the most recommended methods and experimental practice, the supercapacitor cell performance of these porous carbon materials was evaluated and compared in two typical electrolytes: aqueous KOH and organic 1-butyl-3-methylimidazolium tetrafluoroborate (BMIMBF$_4$)/acetonitirle (AN). A clear relationship between SSA and heteroatom on specific capacitance of porous carbon materials was established for these porous carbon materials. In aqueous electrolyte, a balance between Brunauer-Emmett-Teller (BET) SSA and heteroatom of activated porous carbon would be found to develop a supercapacitor with high energy density. For example, porous carbon, obtained at a middle activation temperature (600 °C), shows the largest capacitance value (332 F/g, 0.5 A/g) in aqueous KOH electrolyte corresponding to a medium BET SSA value (1771 m^2/g) and acceptable heteroatom content (N: 1 wt%, O: 8.4 wt%). In organic electrolyte, the capacitance performance of porous carbon was strongly dependent on BET SSA. At the high activation temperature of 800 °C, the corresponding a-CP with maximum BET SSA value (3295 m^2/g) exhibited the maximum capacitance value of ~155 F/g at the current density of 1 A/g. The results provided some insight into potential increase of capacitance performance for porous carbon with considerable heteroatom content in aqueous and organic electrolytes.

2 Materials and methods

The PANi nanorods were synthesized by oxidative polymerization of aniline with ammonium per-sulfate in an aqueous solution containing citric acid according to Yin *et al.*'s report [42]. PANi nanorods were first pyrolyzed at 800 °C for 1 h under argon atmosphere to obtain carbonated PANi (denoted as CP). KOH activation of CP is as follows: typically, 0.5 g of CP was impregnated with 3 g KOH in aqueous solution by sonication followed by evaporation at 80 °C under vacuum. The dried CP/KOH mixtures were also heated at different temperatures ranging from 400 to 800 °C for 1 h under an argon atmosphere. After cooled down to room temperature, the samples were washed with 1 mol/L HCl solution and ultra-pure water until a pH value of 7 was reached. Then, the samples were dried at 60 °C in air. The final activated carbonated PANi products were designated as a-CP-*x*, where *x* represents the activation temperature.

Field emission scanning electron microscopy (FESEM, JSM 6701F, JEOL, Japan) was employed to investigate the surface morphologies of as-prepared porous carbons. Transmission electron microscopy (TEM, 2100 FEG, JEOL, Japan) operated at 300 kV was used to observe the as-prepared carbon structure and morphology. The surface chemical species of the as-prepared carbon was examined by X-ray photoelectron spectroscopy (XPS) using a Perkin-Elmer PHI-5702 multifunctional photoelectron spectrometer (Physical Electronics, Chanhassen, USA) with 1486.6 eV radiation as the excitation source. The chemical compositions of these carbon samples were analyzed by Fourier transformation infrared spectroscopy (FTIR) using a IFS66V FTIR spectrometer (Bruker, Germany). The nitrogen adsorption-desorption isotherm measurements were performed on an ASAP 2020 volumetric adsorption analyzer (Micromeritics, USA) at 77 K. The BET method was used to calculate the SSA. The PSD was derived from the adsorption branch of the corresponding isotherm using the Barrett-Joyner-Halenda method. The total pore volume was estimated from the amount adsorbed at a relative pressure of $P/P_0 = 0.99$.

Electrochemical measurements were carried out using an electrochemical workstation (CHI660D, Shanghai, China) in a two-electrode system at room temperature. For aqueous

cell system, 2 mol/L KOH aqueous solutions were used as electrolyte. The working electrodes were prepared as follows: 90 wt% of sample was mixed with 5 wt% of acetylene black in an agate mortar until a homogeneous black powder was obtained. To this mixture, 5 wt% of poly(tetrafluoroethylene) was added with a few drops of ethanol. After the solvent was briefly allowed to evaporate, the resulting paste was pressed at 10 MPa to the 12 mm diameter nickel foam which served as the current collector. Each electrode contained about 2–3 mg of electro-active material. The electrode was dried for 10 h at 60 °C in air. The electrodes were assembled into coin cell (2032) and separated by a porous nonwoven cloth separator. For organic electrolyte cell system, $BMIMBF_4$/AN (mass ratio of 1:1) was used as electrolyte. The working electrodes were prepared as follows: 90 wt% of sample was mixed with 5 wt% of acetylene black and 5 wt% PTFE in an agate. Then, the mixture was rolled into 30–50 μm thickness sheets and cut into 10 mm × 10 mm electrodes. A pair of typical electrodes had a weight between 4 and 6 mg after drying over-night at 160 °C under vacuum. The dry electrodes were transferred into a glove box filled with Ar to assemble two-electrode symmetrical supercapacitor, which consisted of two current collectors (aluminum foils), two electrodes and a porous separator (Ceglard 3501) sandwiched in a coin cell (2032) consisting of two stainless steel meshes.

All the electrochemical tests were carried out at room temperature. Average specific capacitance values were calculated from the galvanostatic discharge curves, using the following equation:

$$C = 4I / [(\mathrm{d}E / \mathrm{d}t) \times m] \approx 4I / [(\Delta E / \Delta t) \times m] \ (F / g) \quad (1)$$

where I is a constant discharge current, Δt is the time period for a full discharge, m indicates the mass of the corresponding active electrode material, and ΔE represents the voltage change after a full discharge.

3 Results and discussion

Porous carbon rods were prepared by oxidative polymerization, followed by pyrolysis and chemical activation under different temperatures (Figure 1(a)). The SEM image (Figure 1(b)), TEM image (Figure 1(c)), and annular dark field scanning TEM (ADF-STEM) image (Figure 1(d)) showed the rod morphology of a-CP sample. Figure 1(e, f) exhibited the high-resolution ADF-STEM and TEM images of the microstructure, respectively. These images clearly indicated that KOH activation process preserved the rod morphology with the diameter ranging from 100 to 150 nm and had generated a substantial amount of micro/mesopores that were homogeneously distributed throughout the rod-like microstructure.

Most of the activation parameters (activation temperature, mass ratio of hydroxide to precursor, and activation time) could affect the BET surface area and pore structure of porous carbon [19, 20, 22, 43]. Some studies showed that the

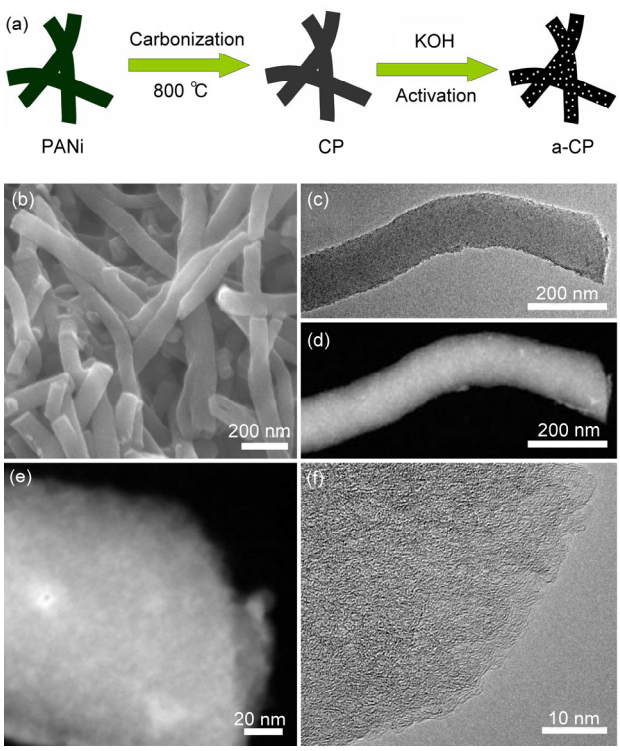

Figure 1 (a) A schematic show of the facile process of synthesizing PANi-derived porous carbon rods; (b~d) SEM image, TEM image, and annular dark field scanning TEM (ADF-STEM) image, showing the typical rod morphology of as-prepared porous carbon; (e, f) high resolution ADF-STEM image and TEM image of porous carbon rod.

activation temperature was the simple and effective way to control the BET surface area of activated carbon [19, 22]. Figure S1(a) shows the dependence of BET surface area on activation temperature. The BET surface area of a-CP gradually increased from 252 to 3295 m^2/g with an increase in activation temperature from 400 to 800 °C, and the corresponding pore volumes rapidly increased. Also, the gradual increase of adsorbed volume in nitrogen isotherm curves indicated the significant impact of activation temperature on their porosity (Figure 2(a)). A noticeable emergence of mesopores could be obtained at relatively high activated temperatures (above 700 °C, Figure 2(b)), which was similar to the polypyrrole-derived activated carbon [22].

XPS was performed to characterize the effect of activated temperature on the element composition of a-CP sample. XPS analyses (Figure 2(c)) showed that CP and a-CP samples were majorly composed of carbon, oxygen, and nitrogen elements, indicating some heteroatom (O and N) groups existing in a-CP samples. The gradually increased activated temperature would push down the N content in a-CP sample to less than 1 wt% (Figure S2(a, b)). The fitting of N1s peaks for CP suggested the existence of three contributions at binding energies of 397.9, 400.5, and 403 eV (Figure S2(c)). These peaks could be assigned to pyridine, quaternary, and oxidized nitrogen, respectively [25]. The N1s core level peaks for a-CP-400 and a-CP-500 samples showed

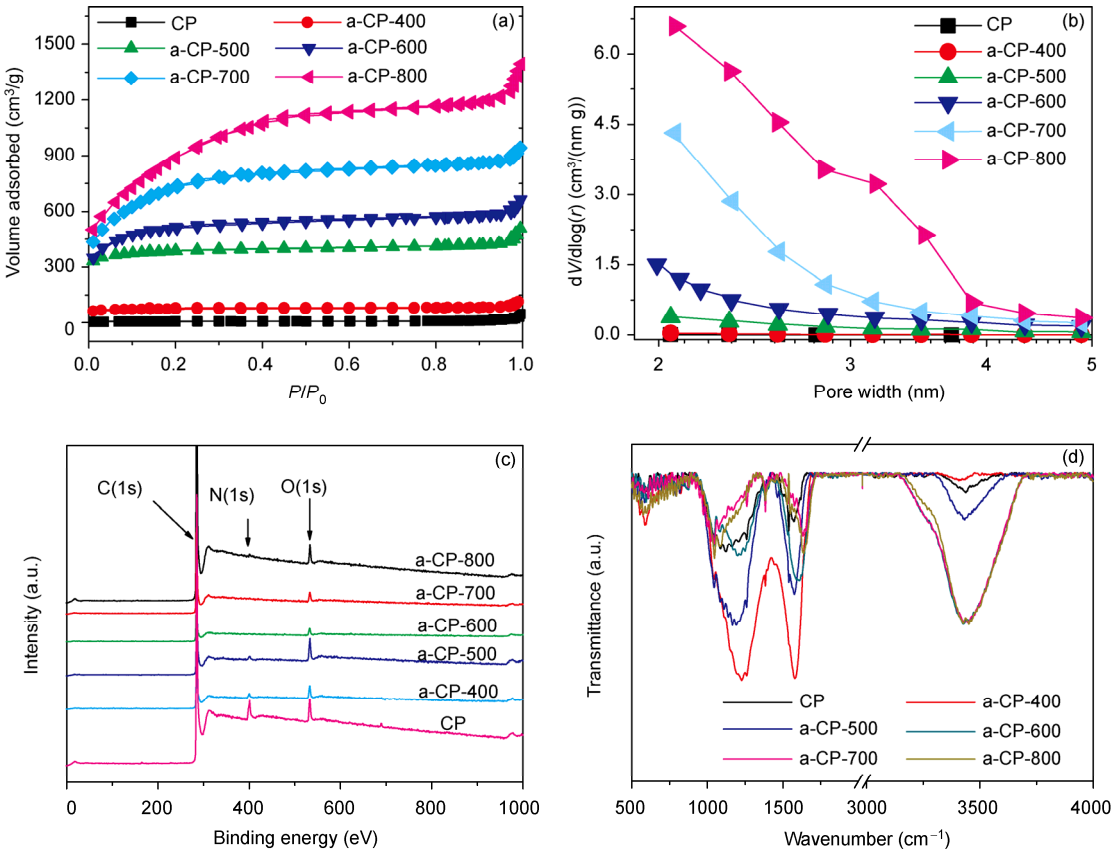

Figure 2 The N_2 sorption isotherm curves (a), PSD (b), XPS spectra (c), and FTIR spectra (d) of CP and a-CP samples activated at different temperatures.

similar shapes to that of CP. However, these N1s disappeared at high activation temperature (> 500 °C). However, O content was enriched in a-CP-400 with ~12.5 wt% relative to the pristine CP with ~3.6 wt%, which indicated that a pre-oxidation may occur in the initial KOH activation stage. With a further increase of activated temperature, the oxygen content fell off. Only about 3.25 wt% O was detected in a-CP-800 sample. Also, FTIR analyses confirmed a tendency that O content increased first and then decreased. The remarkable increase of broad peaks at 1000–1400 and 1500–1700 cm^{-1} for a-CP-400 and a-CP-500 samples respectively in Figure 2(d) indicates the expansion of carboxylation on the surface after KOH activation at 400 and 500 °C. It was interesting to note that the intensity of this band (3200–3700 cm^{-1}) increased as the activated temperature was over 600 °C. This band can be assigned to the adsorbed H_2O. Previous studies showed that carbon materials with the high BET surface areas had a strong ability to adsorb H_2O [44]. These results shown in Figures 2 and S2 indicates that a-CP sample synthesized in the temperature range studied had the increased BET SSA and decreased heteroatom content of activated carbons, making it a good model system to study the effect of BET SSA and heteroatom on electrochemical capacitance.

To clarify the influence of BET SSA and surface heteroatom functionalities on the supercapacitor performance of CP and a-CP samples, two typical electrolytes (aqueous KOH and organic $BMIMBF_4$/AN) were employed. Figure 3(a, b) shows the electrochemical performance of CP and a-CP symmetrical supercapacitor in aqueous KOH solution within the potential range of 0–1 V. For non-activated CP sample cell, cyclic voltammetry (CV) curve was not square from 0 to 1 V and the slope was present, indicating its relatively low capacitance performance (Figure 3(a)). For a-CP sample cells, CV curves (Figure 3(a)) tended to rectangular shape at the scan rate of 100 mV/s and charging/discharging curves (Figure 3(b)) shifted to symmetrical and linear in total potential range, indicating the typical capacitance behavior of carbon materials. Figure 3(c, d) shows the electrochemical performance of CP and a-CP symmetrical supercapacitor in ionic liquid $BMIMBF_4$ and AN mixed electrolyte. CV curves of a-CP sample cells tended to rectangular shape at the scan rate of 100 mV/s and charging/discharging curves shifted to symmetrical and linear in total potential range 0–3.5 V with the elevated activation temperature. Especially, the optimal rectangular CV and linear charge/discharge curves were observed in a-CP-800 cell. For CP cell, it showed the relatively low capacitance values both in KOH and $BMIMBF_4$/AN electrolyte (Figure S3). With an increase of activation temperature, the capacitance values of a-CP cells increased first and then decreased in KOH electrolyte (Figure S3 and Table 1). At 600 °C, the

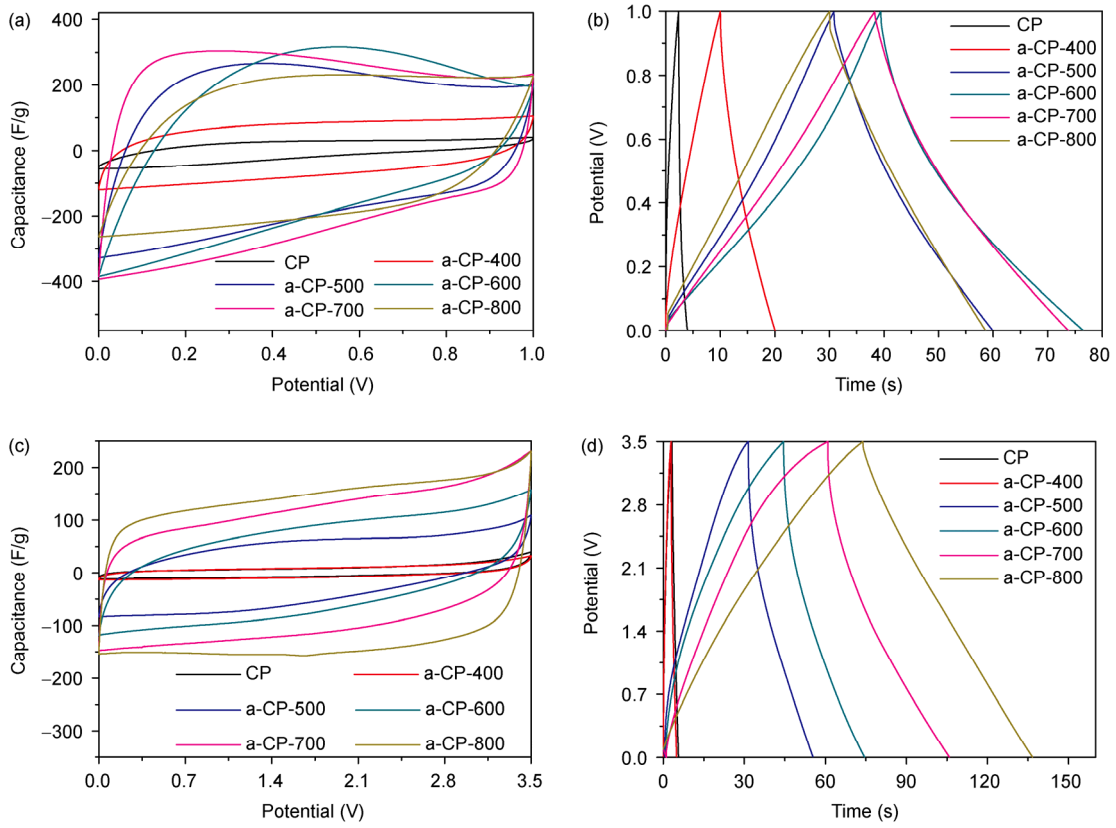

Figure 3 Electrochemical characteristics of the CP and a-CP samples activated at different temperatures in different electrolytes under the two-electrode cell system. In aqueous (KOH) electrolyte: (a) CV curves at the scan rate of 100 mV/s; (b) galvanostatic charge/discharge curves at the current density of 1 A/g. In organic ($BMIMBF_4$/AN) electrolyte: (c) CV curves at the scan rate of 100 mV/s; (d) galvanostatic charge/discharge curves at the current density of 1 A/g.

Table 1 Summary of pore structure, elemental composition, and capacitance values of CP and a-CP samples

Samples	S_{BET} [a] (m^2/g)	S_{micro} [a] (m^2/g)	V_p [a] (cm^3/g)	O [b] (wt%)	N [b] (wt%)	C_{Fa} [c] (F/g)	C_{Fo} [d] (F/g)	C_{sa} [e] (μF/cm^2)	C_{so} [e] (μF/cm^2)
CP	21	13	0.03	3.55	6.37	25	117	6	30.6
a-CP-400	253	209	0.14	12.49	3.06	95	37.8	6	25.1
a-CP-500	1297	1053	0.68	11.26	3.13	246	19	68	5.3
a-CP-600	1771	1085	0.92	8.41	1.04	315	17.8	91	5.1
a-CP-700	2532	487	1.36	5.42	0.22	301	11.9	126	5
a-CP-800	3295	–	1.92	3.21	0.67	240	7.3	155	4.7

a) Obtained from N_2 adsorption-desorption isotherm; b) quantified by XPS; c) C_{Fa} represents capacitance value derived from aqueous KOH solution; d) C_{Fo} represents the capacitance value derived from organic $BMIMBF_4$/AN electrolyte; e) C_{sa} and C_{so} (obtained by dividing the specific capacitance value by BET SSA) represents the normalized capacitance values in aqueous KOH and organic $BMIMBF_4$/AN electrolyte, respectively

maximum capacitance value of ~315 F/g could be obtained, although the BET SSA of a-CP-600 sample only had 1771 m^2/g. For a-CP-800 sample, its BET SSA increased to 3295 m^2/g. However, only 240 F/g could be obtained. In $BMIMBF_4$/AN electrolyte, the capacitance values increased with the elevated activation temperature. CP and a-CP-400 showed capacitance values of only ~6.4 and ~6.3 F/g, respectively. At the high activation temperature of 800 °C, the corresponding a-CP cell exhibited the maximum capacitance value of ~155 F/g at the current density of 1 A/g.

Table 1 shows that the capacitance properties of a-CP cells which exhibit different trends with the elevated activation temperature in these two electrolytes. The different trends were particularly interesting because BET SSA played an important role in determining the capacitance performance of a-CP sample in $BMIMBF_4$/AN electrolyte, while a similar relationship for a-CP samples was not observed in aqueous KOH electrolyte. Some other factors should be considered. As we know, the capacitance was mainly contributed from two parts: EDLC from charge adsorption and pseudocapacitance from redox reactions [28–30]. From XPS and FTIR analyses (Figure 2(c, d)), heteroatom (O and N) contents in carbon materials changed with the elevated activation temperature. The redox actions of electrochemically

active heteroatom (N or O) functionalities on carbon surface brought in the additional pseudocapacitance in aqueous KOH electrolyte. Although CP enriched with 6.37 wt% N, poor capacitance performance of CP was observed. This was due to the non-porous structure of CP and the low utilization of N heteroatoms. At a low activation temperature, a-CP-400 was enriched with 12.5 wt% O and 3 wt% N followed by BET SSA value increasing from 20.9 m^2/g for CP to 252.8 m^2/g, and the corresponding capacitance value increased by 290%, from 24.5 F/g for CP to 95.4 F/g. The pre-oxidation effect in initial KOH activation increased the O atom content on the surface of carbon rods. The additional O atoms contributed to the capacitance performance of a-CP-400 as the form of pseudocapacitance. However, the capacitance value for a-CP-400 did not increase in $BMIMBF_4$/AN electrolyte. The additional O functional groups might not have additional pseudocapacitive contribution which was different from N functional groups in organic electrolyte. Also, according to Zhang *et al.*'s effective SSA model [19], an effective EDLC might not form on the newly developed pore in a-CP-400. This was mainly because that the diameter of newly formed pore was less than $BMIM^+$ (1.11 nm).

With an increase of the activation temperature from 400 to 600 °C, the O and N contents in a-CP sample decreased to 8 wt% and 1 wt% (Figure S2(a)), respectively. However, the-BET SSA increased from 252 to 1771 m^2/g (Figure S1(a)) and the capacitance value shifted to the maximum value of 315 F/g (1 A/g, Table 1) in KOH electrolyte. With an increase of the activation temperature from 600 to 800 °C, BET SSA of a-CP samples continued to increase. However, the capacitance and heteroatom (N and O) contents decreased. Traditionally, the gradual formation of pore structure on carbon rod could enable the formation of a larger number of double layers to facilitate the transport of electrolyte ions, hence providing an enhanced capacitance performance. Also, with regard to the reduced heteroatom content in a-CP sample, pseudocapacitance from heteroatom functional groups decreased. Due to that, a-CP-600 sample obtained the maximum capacitance value. For $BMIMBF_4$/AN electrolyte system, the capacitance values of a-CP samples gradually increased with the elevated activation temperature. When the activation temperature increased, the micropore in a-CP formed and evolved to mesopore as indicated: the S_{micro} value increased from a lower value of 13 m^2/g for CP to a higher value of 1085 m^2/g for a-CP-600, and then decreased for a-CP-700/800 samples (Table 1). Pore distribution further proved a gradually increased mesopore in a-CP sample with the elevated activation temperature (Figure 2(b)). Although micropore generated in a-CP-500 and a-CP-600 sample, the diameter of newly formed micropore may be less than that of $BMIM^+$ (1.11 nm), which results in the lower capacitance values of a-CP-500 and a-CP-600 samples. For a-CP-700/800 sample, large amount of mesopores are generated (Table 1 and Figure 2(b)), which facilitated $BMIM^+$ ion to enter into the pore and enabled the formation of effective double layers to store the charge.

For further study, we summarized the specific capacitance normalized by BET SSA, as shown in Table 1. Different trends were obtained. In aqueous KOH electrolyte, CP sample exhibited the maximum C_s value of 117 $\mu F/cm^2$. After the initial KOH activation process (400 °C), a-CP-400 was enriched with ~12.5 wt% O (Figure S2(a)), but the C_s values decreased dramatically from 117 to 37.7 $\mu F/cm^2$. Meanwhile, 3 wt% N was lost in this stage. This result indicated that pseudocapacitance contribution from N heteroatom groups may be larger than that of O functional groups. With the elevated activation temperature from 400 to 800 °C, the C_s values decreased gradually from 37.7 to 7.3 $\mu F/cm^2$, although the total capacitance increased dramatically from 95.4 to 240 F/g. Considering the quasi-rectangular CV (Figure 3(c)), vertical-like charging/discharging (Figure 3(d)), and low heteroatom content (Figure S2(a)) of a-CP-800, the C_s value of a-CP-800 is majorly contributed from EDLCs without significant pseudocapacitance from Faradaic interactions. Hence, C_s values gradually decreased in aqueous electrolyte, which were majorly related to the decrease of heteroatom content in a-CP samples with the increase of activation temperature. In organic electrolyte, CP sample also had the maximum C_s value of 19.6 $\mu F/cm^2$. This value was obviously lower than the C_s value (117 $\mu F/cm^2$) in aqueous KOH electrolyte but higher than other experimental/theoretical value (4–14 $\mu F/cm^2$) in organic electrolyte [13, 19]. This result indicated Faradaic interactions existed in heteroatom-enriched carbon materials under such an organic environment, which was less significant than that observed in aqueous electrolytes. An enhanced capacitance from N-enriched carbon in an organic electrolyte had also been reported by other researchers [25, 34]. When compared to CP (19.6 $\mu F/cm^2$) and a-CP-500 (5.2 $\mu F/cm^2$), a-CP-400 was enriched with 12.5 wt% O, and the corresponding C_s value reduced to a lower value of 2.1 $\mu F/cm^2$. This reverse trend suggested that the newly formed pore had no apparent capacitive contribution and additional O groups appeared to have a detrimental effect on the normalized capacitance in $BMIMBF_4$/AN electrolyte. The difference between N and O pseudocapacitance contributions in aqueous and organic electrolytes is evident, but its mechanism remains unclear. Since the higher activation temperature was larger than 400 °C, the C_s values of a-CP samples could be stabilized at ~4.9 $\mu F/cm^2$ with no significant reduction. The results suggested that increasing the BET surface area and cutting down heteroatom functional groups both had no significant influence on the C_s value in this stage.

Although the significant capacitance improvement in activated samples and the high C_s value observed in CP samples are an evident consequence of pseudocapacitance in both aqueous KOH and organic $BMIMBF_4$/AN electrolytes,

the mechanisms by which the pseudocapacitance occurs are clearly different, as evidenced by the gradually increased BET SSA and changed heteroatom contents. When a-CP-400 was enriched with 12.5 wt% O and lost with 3.3 wt% N, the capacitance values increased from 25 to 95 F/g in aqueous electrolyte compared with no change in capacitance values in organic electrolyte. Also, the corresponding C_s value in organic electrolyte reduced to a lower value of 2.1 μF/cm^2 when compared with CP (19.6 μF/cm^2) and a-CP-500 (5.2 μF/cm^2). Some conclusions can be drawn from these results and other works. First of all, the pseudocapacitance in aqueous KOH medium was due to redox reactions of electrochemically active functional groups on the carbon surface. According to the works of Hulicova-Jurcakova *et al*. [35] and Chen *et al*. [45, 46], we proposed redox reactions of oxygen and nitrogen functionalities in aqueous KOH electrolytes as shown in Figure 4(a). In addition to organic BMIMBF$_4$/AN electrolyte, oxygen groups may not induce the redox reaction and bring the additional pseudocapacitance contribution. The most reactive redox reactions in organic BMIMBF$_4$/AN electrolyte were generated from nitrogen groups, and the corresponding redox mechanisms are proposed in Figure 4(b). It should be noted that the as stated above reaction mechanism is not rigorously confirmed. Further works are still needed to clarify the different heteroatom effect on the electrochemical capacitance performance of carbon, especially in organic electrolyte.

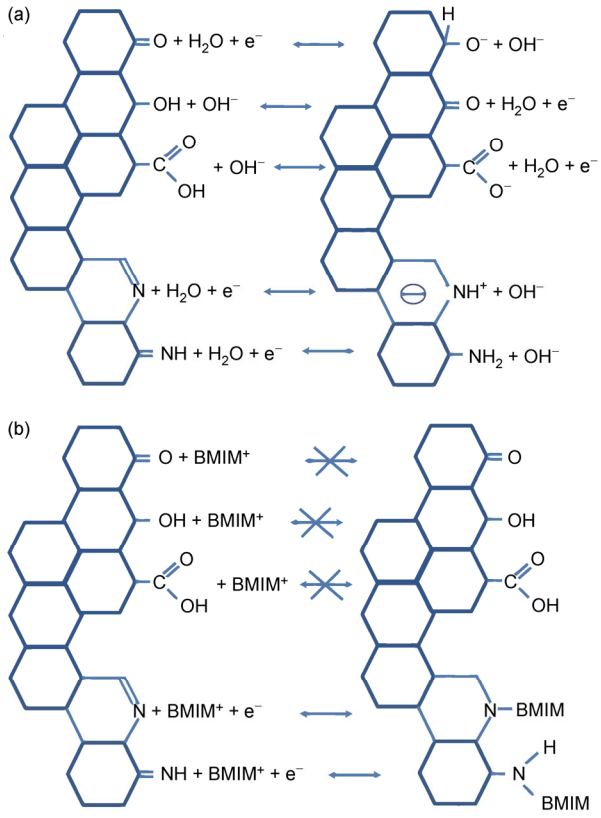

Figure 4 The schematic of the proposed reversible pseudocapacitive reactions of heteroatom functional groups (N and O) in aqueous KOH (a) and organic BMIMBF$_4$/AN (b) electrolytes, respectively.

As an ideal supercapacitor, it was expected that carbon materials had two typical characteristics: large BET SSA and high C_s value. From our study, large BET SSA and high C_s value both could not be obtained. BET SSA and C_s value showed different trends with the elevated activated temperature. Recently, some elegant works had dedicated to developing non-porous carbons with high C_s values through introducing heteroatom functional groups on the carbon surface, but the corresponding total capacitances of carbon materials were far below expectation [34, 35]. Therefore, a compromise between BET SSA and C_s would be used to develop a supercapacitor with high energy density. For example, a-CP-600 sample showed the largest capacitance value (332 F/g, 0.5 A/g) in aqueous KOH electrolyte, while it had a medium BET SSA value (1771 m^2/g) and acceptable heteroatom content (N: 1 wt%, O: 8.4 wt%).

Other important factors, such as rate capability and cycle stability, should be considered to fabricate a high performance supercapacitor. The a-CP-600 cell exhibited a rate capability of 50.8% (Figure S3(a)) and cycle stability of 84% (after 5000 cycles, Figure S4), while it was slightly less than a-CP-800-based supercapacitor which had a rate capability of 61.9% and cycle stability of nearly 100%. This would largely account for the reversible redox action from heteroatom functional groups which did not work effectively and stably at high or long current loads [3, 47, 48]. Pandolfo *et al.* [3] suggested that heteroatom functional groups, which can catalyze the electrochemical oxidation or reduction of the carbon, or the decomposition of the electrolyte components, lead to increase of leakage current, gas generation, and equivalent series resistance. Thus, a strategy which combined the reduced proportion of pseudocapacitance from heteroatom functional groups and the increased effective BET SSA of carbon materials should be considered to fabricate a supercapacitor with high power density and cycle stability. In organic electrolyte, the pseudocapacitance contributed from heteroatom functional groups was obviously less than that in aqueous electrolyte. A richer O heteroatom had a detrimental effect on the capacitance performance in organic electrolyte as observed in a-CP-400 sample, although its mechanism remained unclear. Although, high heteroatom content in a-CP sample went against the rate ability and cycle stability of supercapacitor. As shown in Figure 3, non-rectangle CV curves and non-vertical discharging lines of a-CP samples were observed at the low activation temperatures. Figure S3(b) shows that a-CP-800 cell has the higher rate capability (~74.8%) than that of other a-CP cells. The cycle stability test (Figure S5) also showed that a-CP-600 maintains only 39% of the initial capacitance after 1000 cycles which was not as much as 98% of a-CP-800. Also, the capacitance value was linear with BET SSA, which indicated that carbon materials with high BET SSA could achieve high capacitance performance.

Generally speaking, a low heteroatom functional groups and high BET surface area contributed to a supercapacitor with the high capacitance value, desirable rate ability, and excellent cycle stability in organic electrolyte.

4 Conclusions

Controlling of BET SSA and heteroatom content of porous carbon materials had been realized by adjusting KOH activation temperatures. Experimental results show that BET SSA and heteroatom have different effects on the electrochemical capacitance performance of the porous carbon in aqueous KOH and organic $BMIMBF_4$/AN electrolyte. In aqueous KOH electrolyte, the capacitance performance of porous carbon materials is related to two factors: pore structure (BET SSA) and heteroatom content (heteroatom functional groups). High BET SSA can enable the formation of a large number of double layers to enhance energy storage capacity and rate capability, but an obtained high BET SSA is based on high activation temperature. Abound heteroatom functional groups in porous carbon materials introduce the extra pseudocapacitance toward to increase the C_s value, but heteroatom functional groups are not stable at high activation temperature. A balance between BET SSA and heteroatom of KOH activated porous carbon would be found to develop a supercapacitor with high energy density. In organic electrolyte, the capacitance performance of KOH activated porous carbon is strongly dependent on BET SSA. High BET SSA and low heteroatom content should be considered to ensure a supercapacitor combining high energy density and superior power density. Hence, our results can be used to guide the design of porous carbon materials for supercapacitor with the desired capacitive performance in aqueous and organic electrolytes.

This work was supported by the Top Hundred Talents Program of Chinese Academy of Sciences, the National Natural Science Foundation of China (21203223), and the Youth Science Foundation of Gansu Province (1107RJYA274).

1 Winter M, Brodd RJ. What are batteries, fuel cells, and supercapacitors. *Chem Rev*, 2004, 104: 4245–4270
2 Zhai YP, Dou YQ, Zhao DY, Fulvio PF, Mayes RT, Dai S. Carbon materials for chemical capacitive energy storage. *Adv Mater*, 2011, 23: 4828–4850
3 Pandolfo AG, Hollenkamp AF. Carbon properties and their role in supercapacitors. *J Power Sources*, 2006, 157: 11–27
4 Liang CD, Li ZJ, Dai S. Mesoporous carbon materials: synthesis and modification. *Angew Chem Int Ed*, 2008, 47: 3696–3717
5 Miller JR, Outlaw RA, Holloway BC. Graphene double-layer capacitor with ac line-filtering performance. *Science*, 2010, 24: 1637–1639
6 Zhu YW, Murali S, Stoller MD, Ganesh KJ, Cai WW, Ferreira PJ, Pirkle A, Wallace RM, Cychosz KA, Thommes M, Su D, Stach EA, Ruoff RS. Carbon-based supercapacitors produced by activation of graphene. *Science*, 2011, 332: 1537–1541
7 Wang RT, Wang PY, Yan XB, Lang JW, Peng C, Xue QJ. Promising porous carbon derived from celtuce leaves with outstanding supercapacitance and CO_2 capture performance. *ACS Appl Mater Interfaces*, 2012, 4: 5800–5806
8 Jurcakova DH, Kodama M, Shiraishi S, Hatori H, Zhu ZH, Lu GQ. Nitrogen-enriched nonporous carbon electrodes with extraordinary supercapacitance. *Adv Funct Mater*, 2009, 19: 1800–1809
9 Górka J, Jaroniec M. Hierarchically porous phenolic resin-based carbons obtained by block copolymer-colloidal silica templating and post-synthesis activation with carbon dioxide and water vapor. *Carbon*, 2011, 49: 154–160
10 Chen H, Zhang X, Zhang HT, Sun XZ, Zhang DC, Ma YW. High-performance supercapacitors based on a graphene-activated carbon composite prepared by chemical activation. *RSC Adv*, 2012, 2: 7747–7753
11 Wang Q, Yan J, Xiao Y, Wei T, Fan ZJ, Zhang ML, Jing XY. Interconnected porous and nitrogen-doped carbon network for supercapacitors with high rate capability and energy density. *Electrochim Acta*, 2013, 114: 165–172
12 Lv Y, Zhang F, Dou Y, Zhai YQ, Wang JX, Liu HJ, Xia YY, Tu B, Zhao DY. A comprehensive study on KOH activation of ordered mesoporous carbons and their supercapacitor application. *J Mater Chem*, 2012, 22: 93–99
13 Chmiola J, Yushin G, Gogotsi Y, Portet C, Simon P, Taberna PL. Anomalous increase in carbon capacitance at pore sizes less than 1 nanometer. *Science*, 2006, 313: 1760–1763
14 Chmiola J, Largeot C, Taberna PL, Simon P, Gogotsi Y. Desolvation of ions in subnanometer pores and its effect on capacitance and double-layer theory. *Angew Chem Inte Ed*, 2008, 47: 3392–3395
15 Feng G, Cummings PT. Supercapacitor capacitance exhibits oscillatory behavior as a function of nanopore size. *J Phys Chem Lett*, 2011, 2: 2859–2864
16 Huang J, Sumpter BG, Meunier V. Theoretical model for nanoporous carbon supercapacitors. *Angew Chem Int Ed*, 2008, 47: 520–524
17 Kondrat S, Perez CR, Presser V, Gogotsi Y, Kornyshev AA. Effect of pore size and its dispersity on the energy storage in nanoporous supercapacitors. *Energy Environ Sci*, 2012, 5: 6474–6479
18 Wang RT, Yan XB. Superior asymmetric supercapacitor based on Ni-Co oxide nanosheets and carbon nanorods. *Sci Rep*, 2014, 4: 3721
19 Zhang L, Ying X, Zhang F, Long GK, Zhang TF, Leng K, Zhang YW, Huang Y, Ma YF, Zhang MT, Chen YS. Controlling the effective surface area and pore size distribution of sp^2 carbon materials and their impact on the capacitance performance of these materials. *J Am Chem Soc*, 2013, 13: 5921–5929
20 Zhang LL, Zhao X, Ji H, Stoller MD, Lai L, Murali S, Mcdonnell S, Cleveqer B, Wallace RM, Ruoff RS. Nitrogen doping of graphene and its effect on quantum capacitance, and a new insight on the enhanced capacitance of N-doped carbon. *Energy Environ Sci*, 2012, 5: 9618–9625
21 Zhong M, Kim EK, McGann JP, Chun SE, Whitacre JF, Jaroniec M, Matyjaszewski K, Kowalewski T. Electrochemically active nitrogen-enriched nanocarbons with well-defined morphology synthesized by pyrolysis of self-assembled block copolymer. *J Am Chem Soc*, 2012, 134: 14846–14857
22 Sevilla M, Valle-Vigón P, Fuertes AB. N-doped polypyrrole-based porous carbons for CO_2 capture. *Adv Funct Mater*, 2011, 21: 2781–2787
23 Qie L, Chen WM, Wang ZH, Zhao QG, Li X, Yuan LX, Lu XL, Zhang WX, Huang YH. Nitrogen-doped porous carbon nanofiber webs as anodes for lithium ion batteries with a superhigh capacity and rate capability. *Adv Mater*, 2012, 24: 2047–2050
24 Zhao L, Fan LZ, Zhou MQ, Guan H, Qiao S, Antonietti M, Titirici MM. Nitrogen-containing hydrothermal carbons with superior performance in supercapacitors. *Adv Mater*, 2010, 22: 5202–5206
25 Hulicova D, Kodama M, Hatori H. Electrochemical performance of nitrogen-enriched carbons in aqueous and non-aqueous supercapacitors. *Chem Mater*, 2006, 18: 2318–2326
26 Ania CO, Khomenko V, Raymundo-Piñero E, Parra JB, Béguin F. The large electrochemical capacitance of microporous doped carbon obtained by using a zeolite template. *Adv Funct Mater*, 2007, 17: 1828–1836

27 Andreas HA, Conway BE. Examination of the double-layer capacitance of an high specific-area C-cloth electrode as titrated from acidic to alkaline pHs. *Electrochim Acta*, 2006, 51: 6510–6520
28 Seredych M, Hulicova-Jurcakova D, Lu GQ, Bandosz TJ. Surface functional groups of carbons and the effects of their chemical character, density and accessibility to ions on electrochemical performance. *Carbon*, 2008, 46: 1475–1488
29 Jurewicz K, Pietrzak R, Nowicki P, Wachowska H. Capacitance behaviour of brown coal based active carbon modified through chemical reaction with urea. *Electrochim Acta*, 2008, 53: 5469–5475
30 Frackowiak E, Lota G, Machnikowski J, Vix-Guterl C, Beguin F. Optimisation of supercapacitors using carbons with controlled nanotexture and nitrogen content. *Electrochim Acta*, 2006, 51: 2209–2214
31 Qiu YC, Zhang XF, Yang SH. High performance supercapacitors based on highly conductive nitrogen-doped graphene sheets. *Phys Chem Chem Phys*, 2011, 13: 12554–12558
32 Qian WJ, Sun FX, Xu YH, Qiu LH, Liu CH, Wang SD, Yan F. Human hair-derived carbon flakes for electrochemical supercapacitors. *Energy Environ Sci*, 2014, 7: 379–386
33 An BG, Xu SF, Li LX, Tao J, Huang F, Geng X. Carbon nanotubes coated with a nitrogen-doped carbon layer and its enhanced electrochemical capacitance. *J Mater Chem A*, 2013, 1: 7222–7228
34 Hulicova-Jurcakova D, Kadama M, Shiraishi S, Hatori H, Zhu ZH, Lu GQ. Nitrogen-enriched nonporous carbon electrodes with extraordinary supercapacitance. *Adv Funct Mater*, 2009, 19: 1800–1809
35 Hulicova-Jurcakova D, Serdych M, Lu GQ, Bandosz TJ. Combined effect of nitrogen- and oxygen-containing functional groups of microporous activated carbon on its electrochemical performance in supercapacitors. *Adv Funct Mater*, 2009, 19: 438–447
36 Li X, Wang HL, Robinson JT, Sanchez H, Diankov G, Dai HJ. Simultaneous nitrogen doping and reduction of graphene oxide. *J Am Chem Soc*, 2009, 131: 15939–15944
37 Kim YJ, Abe Y, Yanagiura T, Park KC, Shimizu M, Iwazaki T, Nakagawa S, Endo M, Dresselhaus MS. Easy preparation of nitrogen-enriched carbon materials from peptides of silk fibroins and their use to produce a high volumetric energy density in supercapacitors. *Carbon*, 2007, 45: 2116–2125
38 Hulicova D, Yamashita J, Soneda Y, Hatori H, Kodama M. Supercapacitors prepared from melamine-based carbon. *Chem Mater*, 2005, 17: 1241–1247
39 Yan J, Wei T, Qiao WM, Fan ZJ, Zhang LJ, Li TY, Zhao QK. A high-performance carbon derived from polyaniline for supercapacitors. *Electrochem Commun*, 2010, 12: 1279–1282
40 Li LM, Liu EH, Yang YJ, Shen HJ, Huang ZZ, Xiang XX. Nitrogen-containing carbons prepared from polyaniline as anode materials for lithium secondary batteries. *Mater Lett*, 2010, 64: 2115–2117
41 Chen YZ, Zhu HY, Liu YN. Preparation of activated rectangular polyaniline-based carbon tubes and their application in hydrogen adsorption. *Int J Hydrogen Energ*, 2011, 36: 11738–11745
42 Yin JB, Xia X, Xiang LQ, Zhao XP. Conductivity and polarization of carbonaceous nanotubes derived from polyaniline nanotubes and their electrorheology when dispersed in silicone oil. *Carbon*, 2010, 48: 2958–2967
43 Wang J, Chen MM, Wang CY, Wang JZ, Zheng JM. Preparation of mesoporous carbons from amphiphilic carbonaceous material for high-performance electric double-layer capacitors. *J Power Sources*, 2011, 196: 550–558
44 Cuhadaraglu D, Uygun OA. Production and characterization of activated carbon from a bituminous coal by chemical activation. *Afr J Biotechnol*, 2008, 7: 3703–3710
45 Chen CM, Zhang Q, Yang MG, Huang CH, Yang YG, Wang MZ. Structural evolution during annealing of thermally reduced graphene nanosheets for application in supercapacitors. *Carbon*, 2012, 50: 3572–3584
46 Chen CM, Zhang Q, Zhao XC, Zhang BS, Kong QQ, Yang MG, Yang QH, Wang MZ, Yang YG, Schlogl R, Su DS. Hierarchically aminated graphene honeycombs for electrochemical capacitive energy storage. *J Mater Chem*, 2012, 22: 14076–14084
47 Oda H, Yamashita A, Minoura S, Okamoto M, Morimoto T. Modification of the oxygen-containing functional group on activated carbon fiber in electrodes of an electric double-layer capacitor. *J Power Sources*, 2006, 158: 1510–1516
48 Ruiz V, Blanco C, Granda M, Santamaría R. Enhanced life-cycle supercapacitors by thermal treatment of mesophase-derived activated carbons. *Electrochim Acta*, 2008, 54: 305–310